Critical exponents and phase transition in gold nuclei fragmentation at energies 10.6 and 4.0 GeV/nucleon

D. Kudzia, B. Wilczyńska, and H. Wilczyński*
Institute of Nuclear Physics, Radzikowskiego 152, 31-342 Kraków, Poland
(Received 24 September 2002; revised manuscript received 6 June 2003; published 26 November 2003)

An attempt to extract critical exponents γ, β, and τ from data on gold nuclei fragmentation due to interactions with nuclear emulsion at energies 4.0*A* GeV and 10.6*A* GeV is presented. Based on analysis of Campi's second charge moments, two subsets of data at each energy are selected from the inclusive data, corresponding to "liquid" and "gas" phases. The extracted values of critical exponents for the selected datasets are in agreement with predictions of the three-dimensional Ising universality.

DOI: 10.1103/PhysRevC.68.054903 PACS number(s): 25.70.Pq, 05.70.Jk, 24.10.Pa, 21.65.+f

I. INTRODUCTION

Multifragmentation, a breakup of an excited nucleus into many intermediate mass fragments, has been discussed for almost 20 years in terms of statistical mechanics; possible critical behavior was investigated. In its ground state nuclear matter behaves like a liquid. Mean field theory simulations [1] predict that nuclear equation of state resembles that of van der Waals gas. Therefore existence of a phase transition, spinodal instabilities, and a critical point are expected. However, the nature of the possible phase transition is still under debate. Existing experimental data do not lead to a conclusive answer [2–5].

In many papers it was shown (e.g., Ref. [3]) that nuclear interactions undergo two stages. During the first stage, prompt nucleons are emitted from the colliding system and they carry out a large amount of available kinetic energy. They result from quasielastic and nonelastic collisions of projectile and target nucleons. Immediately after the collision, the remnant of the nucleus is in an excited state with temperature T_i. At the second stage, the excited remnant expands and cools evolving into a neighborhood of the critical point on the temperature-density plane [6]. Then it breaks up into many intermediate mass fragments and freezes out at temperature T_f. This last process is the multifragmentation. It was also shown that the total charged fragment multiplicity is proportional to the temperature of the colliding system, both to T_i and T_f [6].

In the 1990's there were many attempts to extract critical exponents in nuclear fragmentation from the experimental data, e.g., Refs. [7–10]. A method of charged moments invented by Campi [11] and supported by percolation theory [12] was commonly applied. These attempts did not take into account the fact that it is only the remnant of the nucleus that undergoes multifragmentation process, so all prompt particles (participating in the nucleus-nucleus collision) were included in the analysis. This approach raised a critique [13,14], that pointed out that: inclusion of prompt particles, assumption that fragment multiplicity is directly proportional to the temperature of the fragmenting system, and using fragment charges Z_i instead of fragment masses A_i are not justified and can significantly change the resulting values of critical exponents.

Recently, the EOS Collaboration [15] calculated critical exponents based on a high-statistics sample of fully reconstructed events from fragmentation of Au nuclei with energy 1.0 GeV/nucleon, taking into account the above criteria and using fragment masses, not charges. The obtained results are in agreement with the previously extracted values of the critical exponents [7]. Therefore, the exclusion of prompt particles and performing analysis based on moments of mass distribution, instead of charge distribution, does not impact resulting values. This can be understood based on the fact that a large majority of prompt particles are fragments with charge $Z=1$. Their impact on the second charge moments (that take square of the charges) is much smaller than that of heavier fragments.

In this paper we present the analysis of data coming from interactions of projectile gold nuclei with nuclear emulsion at primary energies 4.0 and 10.6 GeV/nucleon.

II. THE EXPERIMENT

Stacks of BR-2 emulsion pellicles were irradiated with gold ion beam at the AGS accelerator at Brookhaven National Laboratory. The stacks were oriented so that the beam was parallel to the pellicles. Interactions were found during a microscope scanning along the primary tracks in order to obtain a sample with minimum detection bias. The two datasets consist of 448 events at 4.0 GeV/nucleon and 884 events at 10.6 GeV/nucleon. In each event analyzed, multiplicities and emission angles of all produced particles and fragments of colliding nuclei were measured. In addition, charges of projectile nucleus fragments were determined. Singly charged particles (released protons and produced pions) were distinguished unambiguously from heavier fragments. Charges of heavier fragments ($Z \geqslant 2$) of the projectile were measured using a photometric method with a charge-coupled device camera [16].

The experimental method of identification of prompt particles (i.e., nucleons directly participating in the collision) in emulsion experiments is not available. We can, however, estimate the number of prompt particles as a difference be-

*Electronic address: Henryk.Wilczynski@ifj.edu.pl

tween the total number of emitted protons N_{prot} and the number of spectator protons N_{spec}. The number N_{prot} is determined using charge balance of the projectile fragments. We have estimated N_{spec} as the number of singly charged particles that are emitted at the angle $\theta < 2\theta_0$, where θ_0 is the average proton emission angle given by relation $\theta_0 = 0.12/p$, and p is the momentum per nucleon of the projectile before fragment emission [17].

In this paper critical exponents were extracted using the Campi's charge moment method. The charge moments in our analysis were calculated in two different ways. One of them is to find non-normalized charge moments, taking into account all heavy ($Z > 2$) fragments, α particles, and protons emitted from the vertex of interaction following Gilkes *et al.* [7]. The other way is for normalized charge moments and excludes prompt protons following Elliott *et al.* [15]. The two ways were used to detect possible inconsistencies coming from the choice of the method.

III. CHARGE MOMENTS

Following Campi [11,18], we define the total charged fragment multiplicity m, as $m = N_f + N_\alpha + N_{prot}$, where N_f denotes the number of fragments with charge $Z \geqslant 3$, N_α is the number of emitted α particles, and N_{prot} is the number of emitted protons.

The distance from the critical point for a given event can be properly measured by a difference between multiplicity m and the multiplicity at the critical point m_c. The validity of this assumption rests on a linear dependence between temperature of the system T and the total multiplicity m that was shown to be valid by Hauger *et al.* [3]. Therefore we introduce a variable ϵ:

$$\epsilon = m - m_c. \tag{1}$$

Fragments of a given charge Z_f were counted on event-by-event basis to determine the fragment charge distribution N_{Z_f}. The normalized charge distribution was defined as $n_{Z_f} = N_{Z_f}/Z_{A_0}$, where Z_{A_0} is charge of the nucleus remnant undergoing fragmentation, given by a sum of charges of all fragments $Z_f \geqslant 2$ plus total charge of spectator protons.

In order to compare the experimental results with theoretical calculations based on the Fisher model of droplet condensation [19], which is commonly applied to nuclear fragmentation, mass distributions should be used and should be normalized to the remnant mass A_0 rather than to its charge Z_{A_0}. In emulsion experiments, fragment mass is not measurable; therefore it was assumed that fragment charge Z_f is proportional to its mass A_f. It was also assumed that on average, charge and mass distributions are equal, $N(Z_f) = N(A_f)$. In fact, the same assumption is made also by other authors, at least in specific ranges of charges. This is dictated by the difficulty in measuring masses of all heavier fragments emerging from the interaction vertex. In case of electronic experiments, masses of fragments only in some small mass range are measured. Therefore, we have to rely on the assumption of proportionality between mass and charge.

Following Campi [11], we define the kth moment of charge distribution as

$$M_k(\epsilon) = \sum n_{Z_f}(\epsilon) Z_f^k, \tag{2}$$

where the sum extends over all charged fragments except prompt protons in the "gas phase," that is, for $\epsilon > 0$. In the "liquid phase," where $\epsilon < 0$, in addition the fragment with highest charge Z_{max} is omitted from summation. The above procedure is motivated by the Fisher model: the bulk liquid of infinite volume is excluded from calculation on the "liquid" phase. Similar procedure is carried out in percolation models, in which the percolating cluster of infinite size is excluded from calculation on the liquid phase.

With the above assumptions, and based on the Fisher model, in the thermodynamic limit the following relations are valid [15]:

$$M_2(\epsilon) \sim |\epsilon|^{-\gamma}, \tag{3}$$

$$n_{Z_f}(\epsilon) \sim Z_f^{-\tau} \text{ for } \epsilon = 0. \tag{4}$$

In addition, Bauer *et al.* [20] have shown that

$$Z_{max}(\epsilon) \sim \epsilon^\beta \text{ for } \epsilon < 0. \tag{5}$$

In these equations β, γ, and τ are the critical exponents. $Z_{max}(\epsilon)$ is the average charge of the largest fragment for a given distance from the critical point ϵ. The above relations are valid in the neighborhood of the critical point, provided that the system is at coexistence and the effects of Coulomb energy are relatively small. It was shown in Ref. [21] that these assumptions are approximately valid in nuclear fragmentation, so that the system can be treated as being at coexistence. Far away from the critical point, the behavior of the system is dominated by the mean field regime and these relations are not followed. Very close to the critical point, on the other hand, finite size effects come into play and M_2 does not rise to infinity with ϵ approaching zero [Eq. (3)], but achieves some maximum value. The critical exponents β, γ, and τ are not independent. A scaling relation between them exists:

$$\tau = 2 + \frac{\beta}{\beta + \gamma}. \tag{6}$$

Practical calculations of the moments of charge distributions were based on averaging in the small bins of multiplicity m of event-by-event distributions [15,7]:

$$\langle M_k(\epsilon) \rangle = \frac{1}{N} \sum M_k^i(\epsilon) = \frac{1}{N} \sum_i \left(\sum_{Z_f} n_{Z_f}^i(\epsilon) Z_f^k \right), \tag{7}$$

where i is the index of an event, N denotes the total number of events in a given small range of ϵ, and M_k^i is a charge distribution moment for event i.

IV. FLUCTUATIONS CLOSE TO THE CRITICAL POINT

One of the basic effects of the second-order phase transition is the appearance of significant fluctuations in the neighborhood of the critical point, in a small range of temperatures T (or other parameter measuring distance from the critical point). Fluctuations grow as the critical point is approached

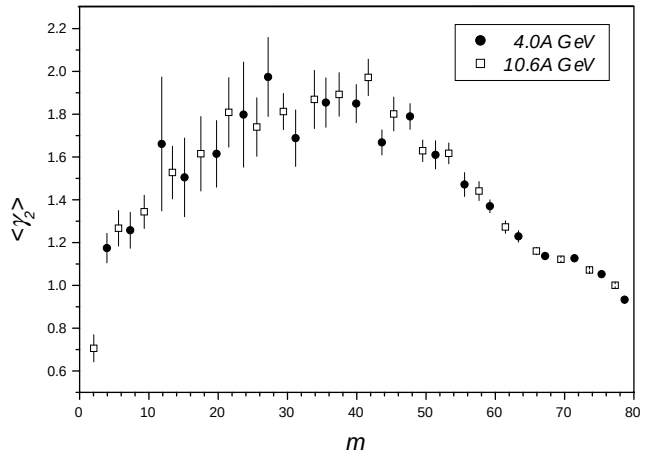

FIG. 1. $\langle\gamma_2\rangle$ as a function of total charged fragment multiplicity m at energies 4.0 and 10.6 GeV/nucleon. The error bars show the dispersion of γ_2 in each bin.

and appear at increasingly large scales. In the case of a normal liquid, the effect is known as the critical opalescence: fluctuations of density of the liquid and sizes of gas bubbles result from vanishing latent heat of the phase transition as the critical point is approached. In the Fisher model applied to nuclear fragmentation, this is reflected by the divergence of the isothermal compressibility κ_T at the critical temperature T_c: small variations of the pressure result in big density changes. In the neighborhood of the critical point, the volume and surface terms of the Gibbs free energy of fragment formation vanish and the fragment distribution is dominated by the power law of Eq. (4).

In case of multifragmentation, fluctuations can be analyzed using moments of charge distributions. Campi suggested a variable γ_2 linearly dependent on variance σ^2 of the charge $\langle Z\rangle$ distribution:

$$\gamma_2 = \frac{M_2 M_0}{M_1^2} = 1 + \frac{\sigma^2}{\langle Z\rangle^2}, \tag{8}$$

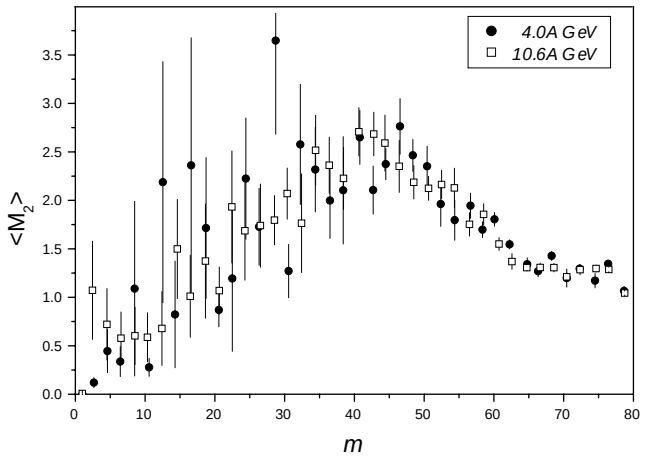

FIG. 2. Mean value of the second charge moment $\langle M_2\rangle$ as a function of multiplicity m for energies 4.0 and 10.6 GeV/nucleon. The error bars show dispersion of M_2 values in each bin.

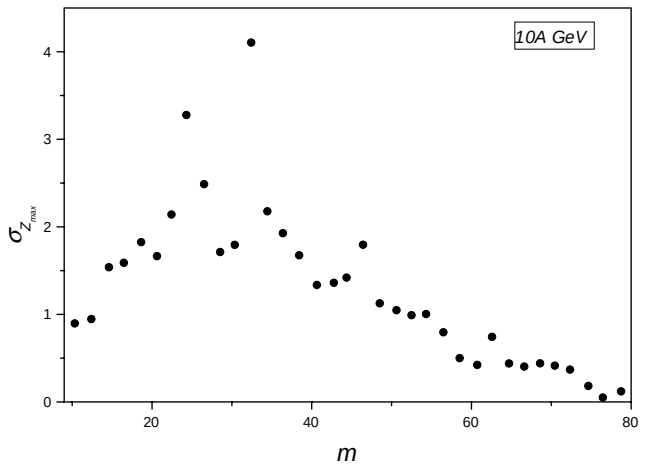

FIG. 3. Standard deviation of Z_{max} as a function of multiplicity m at energy 10.6 GeV/nucleon.

Figure 1 shows $\langle\gamma_2\rangle$ as a function of multiplicity m for energies 4.0 and 10.6 GeV/nucleon. As critical value of multiplicity m_c is not identified at this stage, charge moments were calculated with Z_{max} excluded. For multiplicities smaller than $m\simeq 30$, $\langle\gamma_2\rangle$ grows monotonically with multiplicity, for multiplicities larger than $m\simeq 40$, it falls down monotonically. Fluctuations of γ_2, reflected in large dispersion, are largest for multiplicities between 10 and 40. It is commonly assumed that the strong maximum of $\langle\gamma_2\rangle$ results from undergoing a phase transition at critical point multiplicity $m=m_c$. The region of multiplicities $m<m_c$ is called a liquid phase, and events with $m>m_c$ are called to be in a "gas" phase. However, the presence of maximum of $\langle\gamma_2\rangle$ is not a conclusive argument for appearance of phase transition. It was shown [15] that such maximum is observed also in systems that do not undergo a phase transition. Therefore, Fig. 1 will be treated as only a hint for possible phase transition in a specific range of multiplicities. It is also worth mentioning that γ_2 fluctuations at energies 4.0 and 10.6 A GeV agree well with each other.

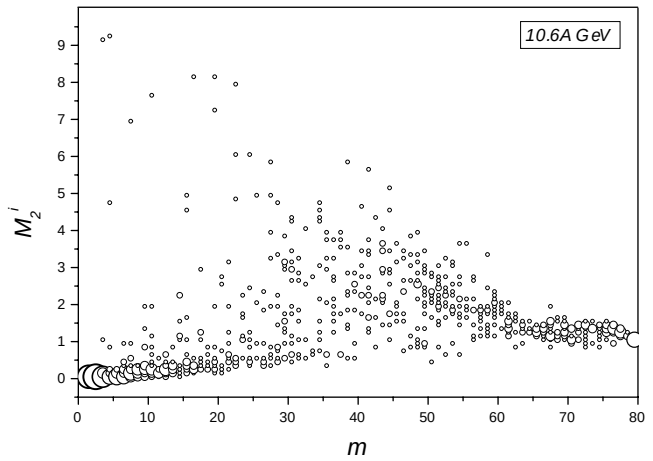

FIG. 4. Scatter plot of second charge moments for individual events M_2^i as a function of multiplicity m at energy 10.6 GeV/nucleon.

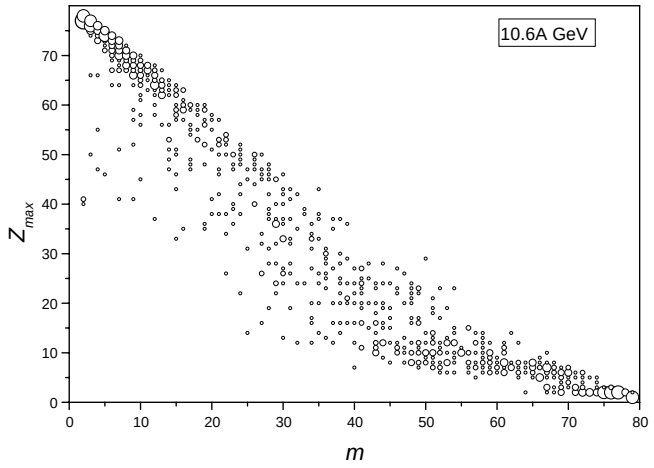

FIG. 5. Scatter plot of charge of the heaviest fragment, Z_{max}, for individual events as a function of multiplicity m at energy 10.6 GeV/nucleon.

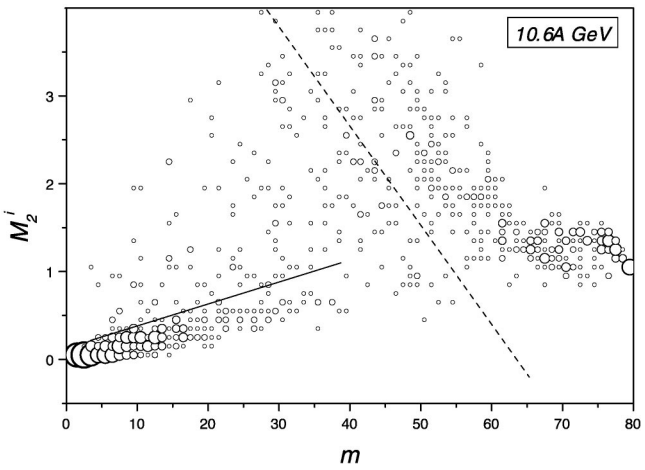

FIG. 6. Selection of liquid and gas groups of events in the M_2^i -m scatter plot.

In order to analyze the fluctuations closer, the mean values of second moment of charge distribution $\langle M_2 \rangle$ were plotted versus multiplicity in Fig. 2. Characteristics similar to that of $\langle \gamma_2 \rangle$ is seen. Large dispersion of M_2, especially in the liquid phase reflects strong fluctuations of experimental values. Also, the Z_{max} distribution exhibits large fluctuations in the m range between about 20 and 40. Figure 3 shows the standard deviation of Z_{max} as a function of m.

Figure 4 shows a scatter plot of second charge moments for individual events M_2^i versus multiplicity m at energy 10.6 GeV/nucleon. Strong fluctuations of M_2^i for multiplicities $15 \leqslant m \leqslant 45$ are clearly visible, which result in large dispersion of M_2 values (shown as error bars in Fig. 2). For systems undergoing a second-order phase transition, it is expected that fluctuations rise in the neighborhood of the critical point. Therefore, observation of large fluctuations quite far away from the expected critical region should be attributed to a different physical phenomenon. For example, events with values of $M_2^i > 4$ and multiplicity $m < 20$ are fissionlike (only two heavy fragments plus α's and protons). Two distinct groups of experimental points are seen in Fig. 4. One of these groups consists of events with multiplicity smaller than $m=35$ and $M_2 < 0.9$, the other—of events with multiplicities larger than $m=30$ and largest M_2 values for a given m. The former group, with small multiplicities and small M_2^i, suggests that the fragment charge distribution must be dominated by one heavy fragment—i.e., the expected characteristics of the liquid phase. On the other hand, the latter group of events, with large multiplicity and larger M_2, suggests existence of a larger number of small fragments; thus it resembles the expected characteristics of the gas phase. The two groups are also clearly distinguishable in Fig. 5, showing the charge distribution of the heaviest fragment, Z_{max}, as a function of fragment multiplicity m. The liquid group can be seen at large Z_{max}, small m region, while the gas group corresponds to small Z_{max}, large m. These two groups were selected from the inclusive experimental data for further analysis on the basis of their second charge moments M_2. Figure 6 shows the selection criteria. The liquid group of events consists of those with multiplicity smaller than $m=35$ located below the solid line, while the gas group consists of events with $m > 30$ and located above and to the right of the dashed line. Similar selection was performed for data at energy 4.0 GeV/nucleon—see Fig. 7. The lines shown in Figs. 6 and 7 were varied around, resulting in slightly different selection criteria. Four different selections were tried to determine the impact of the selection criteria on the resulting values of critical exponents. Each time, the critical exponents obtained were in agreement within statistical errors with the values presented later in this paper.

Let us look at these two selected groups in order to check if they really can be treated as liquid and gas phases. For example, Fig. 8 presents charge distributions as a function of heavy ($Z > 2$) fragment multiplicity N_f for the two selected groups of data. Fragment charge distributions are clearly different in both groups. The charge distribution for the group of low multiplicity events consists mainly of events with one heavy fragment emitted ($Z \geqslant 45$). If the second fragment is emitted, it has a small charge ($Z \leqslant 5$). Therefore, we will refer to this group of data as liquid as for these events one

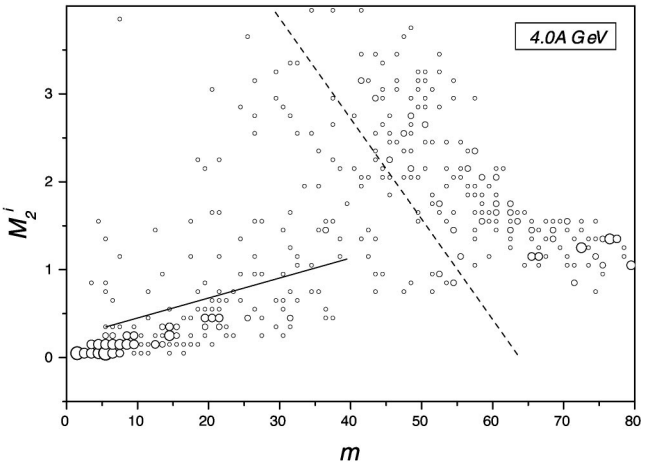

FIG. 7. Second charge moment M_2^i for individual events vs multiplicity m for energy 4.0 GeV/nucleon. Events selection criteria.

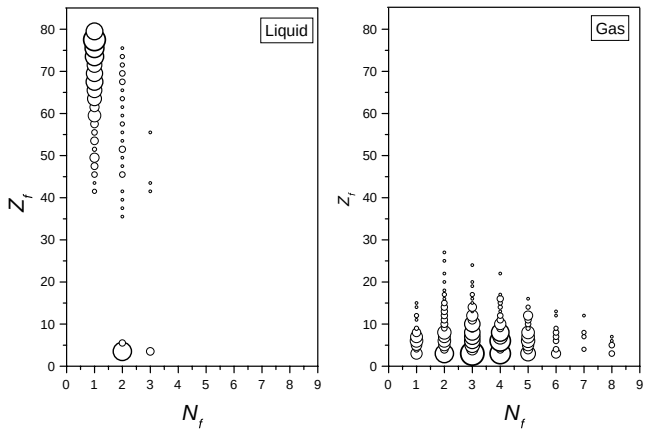

FIG. 8. Charge distributions in events with different heavy fragment multiplicity N_f for the two selected groups of experimental data at energy 10.6 GeV/nucleon.

large fragment remains after collision in analogy to the large drop of liquid. In most cases there are only α's and protons accompanying the large heavy fragment. The second group of events has a totally different charge distribution that consists of events with number of emitted heavy fragments ranging from 1 to 8 and charges of fragments $Z \leqslant 25$. The majority of fragments in this group has charges $Z \leqslant 15$. We will call this group of events a gas as it consists of events with many light fragments emitted. The analysis presented in subsequent sections presents results on these selected sets of data unless explicitly stated otherwise.

V. CRITICAL EXPONENT γ

In order to extract the critical exponent γ and the critical value of multiplicity m_c, the method known as "γ matching" was used [20,15]. The outline of this method is the following. A trial value of the critical multiplicity m_c is chosen. For

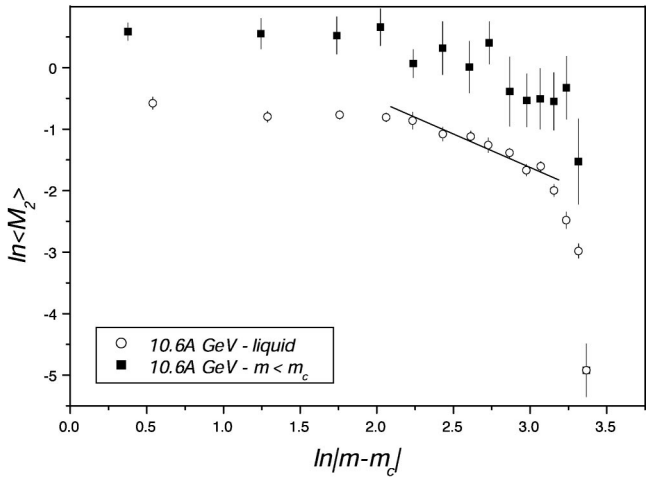

FIG. 9. Mean value of second charge moment $\langle M_2 \rangle$ for the liquid phase as a function of multiplicity m at energy 10.6 GeV/nucleon. Full squares show data for all events with $m < m_c$, and open circles represent data for selected liquid events only. The line shows the fit used to determine critical exponent γ.

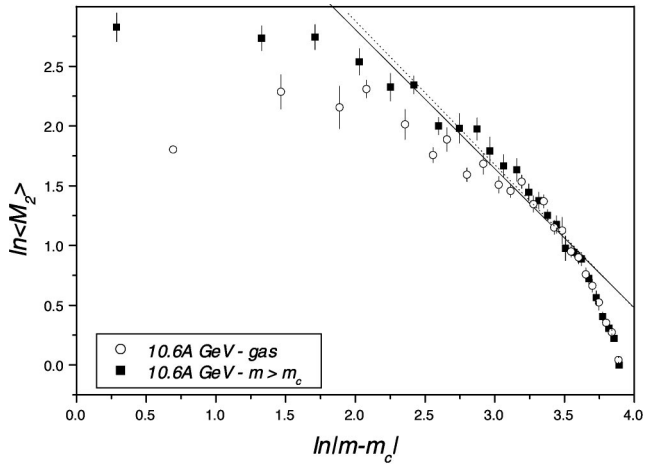

FIG. 10. Mean value of second charge moment $\langle M_2 \rangle$ for the gas phase as a function of multiplicity m at energy 10.6 GeV/nucleon. Full squares show data for all events with $m > m_c$, open circles represent data for selected gas events only. Plotted lines show fits to the gas data (solid line) and $m > m_c$ data (dotted line).

a given m_c, a distribution of mean values of the moment $\langle M_2(\epsilon) \rangle$ is determined as a function of distance from the critical point $\epsilon = m - m_c$. Then the ranges in ϵ are chosen to fit the power law (3) to the experimental data, separately for the gas and liquid phases. With fitting boundaries determined, the linear fit to the $\ln\langle M_2(\epsilon) \rangle$ versus $\ln|\epsilon|$ is made to extract values of the slope γ separately for gas and liquid phases.

The fitting boundaries are determined in the following way. Figure 9 presents a comparison of second moments of charge distribution for the selected liquid phase and all available experimental data at $m < m_c$. It should be noted that we expect that far from the critical point, behavior of the system is dominated by the mean field regime and the power law is not followed. Similarly, very close to the critical point, the finite size effects prevent M_2 from rising to infinity with ϵ approaching zero, and again the power law relation is not valid. These two expected effects are visible in Fig. 9. There-

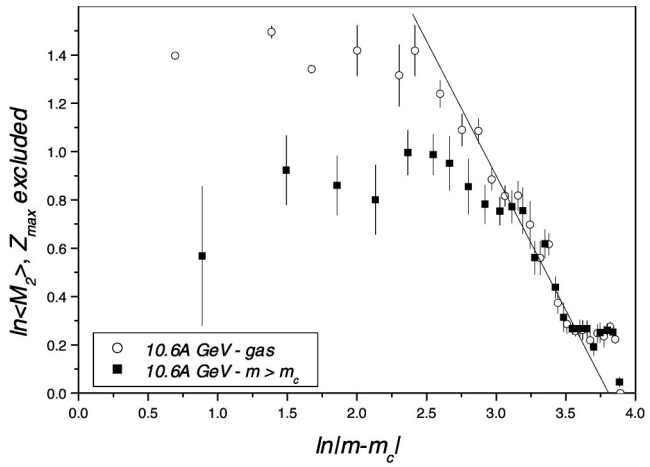

FIG. 11. Mean value of the second charge moment $\langle M_2 \rangle$ for a gas phase with exclusion of the largest charge Z_{max} as a function of multiplicity m for energy 10.6 GeV/nucleon.

TABLE I. Critical exponent γ for gas and liquid phases for different choices of trial value of critical point m_c at energy 10.6 GeV/nucleon used in γ matching procedure. Normalized moments.

Trial m_c	γ_{liquid}	γ_{gas}	$\lvert\gamma_{liquid}-\gamma_{gas}\rvert$
26	0.80±0.00	1.45±0.06	0.63±0.10
28	0.96±0.11	1.32±0.05	0.35±0.12
29	1.04±0.11	1.26±0.05	0.22±0.12
30	1.12±0.12	1.20±0.05	0.08±0.13
31	1.20±0.13	1.14±0.05	0.05±0.14
32	1.27±0.14	1.08±0.05	0.19±0.15
34	1.42±0.15	0.96±0.04	0.46±0.16

fore, if a number of both leftmost and rightmost points in Fig. 9 are to be rejected from calculations, the central region marked by the straight line is a natural choice for the m region to be used in calculating the γ exponent.

Similar comparison for the gas phase is shown in Fig. 10. The impact of selection of the gas phase is not significant in this case. The region of the power law dependence is not clearly seen. This may be due to the inclusion of the charge of the largest fragment Z_{max} in the gas phase. The largest charge dominates the second moment, shifts it to the higher values, and makes the power law less visible, probably due to the finite size effect. Thus, it may be interesting to check if the exclusion of Z_{max} also in the gas phase reveals a clear range of power law dependence of $\langle M_2\rangle$ versus ϵ. The M_2 moment for the gas phase computed without Z_{max} is shown in Fig. 11. Open circles represent moments computed for the gas group of data, and filled circles represent those for all experimental data at $m>m_c$, without selection. In both cases the region of power law behavior can be found. This region is much larger for selected gas data compared to $m>m_c$ data, so it is a reasonable choice for the region of ϵ in which the fit should be performed. In other words, Fig. 11 was used as a guideline in determining fitting region in the gas phase in the γ matching procedure. The value of $\gamma_{gas}=1.14\pm0.05$ determined from moments of charge distribution with Z_{max} excluded is very close to the value determined by the gamma matching procedure (i.e., with Z_{max} included, see below).

The above procedure was repeated for several trial values of the critical point m_c. The value of the critical exponent γ

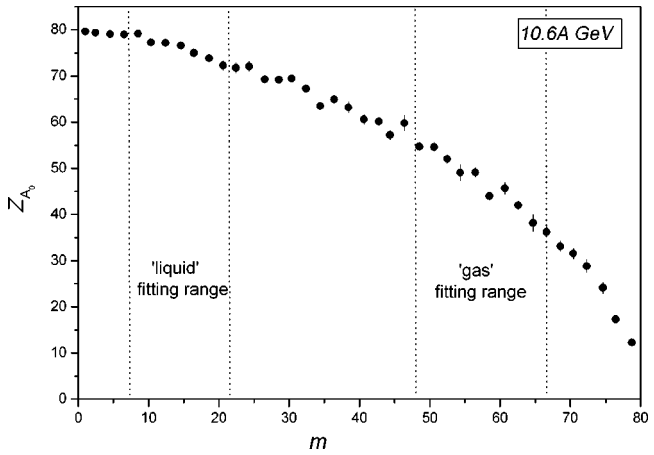

FIG. 12. Mean value of Z_{A_0} as a function of m. The regions of m used in calculation of exponent γ are shown by the dotted lines.

and critical point m_c is found by demanding that $\lvert\gamma_{gas}-\gamma_{liquid}\rvert$ takes a minimum value and γ_{gas} and γ_{liquid} agree with each other within statistical errors. Trial values of the critical point were selected in the range $25\leqslant m_c\leqslant 35$.

Results of the calculations at energy 10.6 GeV/nucleon are presented in Tables I and II. Table I shows results obtained based on normalized charge distribution moments, whereas Table II presents results from calculation based on non-normalized moments. It is seen that both procedures give exponents that agree with each other within statistical errors. The final value of exponent γ is calculated as a mean value of γ_{gas} and γ_{liquid} for normalized moments. The critical point is determined at $m_c=31\pm2$ and the critical exponent $\gamma=1.17\pm0.09$.

It should be noted that calculation of non-normalized moments involves all projectile fragments, while proper evaluation of normalized moments requires that all preequilibrium particles should be removed from the calculation. Thus, these two methods involve summation over different sets of fragments emitted from the collision. As discussed in Sec. III, for normalized moments the charge distribution is normalized by Z_{A_0}, i.e., the charge of the nuclear remnant undergoing multifragmentation. Figure 12 presents Z_{A_0} as a function of fragment multiplicity m, with marked ranges of m used in calculating the critical exponents: $7\leqslant m\leqslant 21$ in the liquid phase

TABLE II. Critical exponent γ for gas and liquid phases for different choices of trial value of critical point m_c at energy 10.6 GeV/nucleon used in γ matching procedure. Non-normalized moments.

Trial m_c	γ_{liquid}	γ_{gas}	$\lvert\gamma_{gas}-\gamma_{liquid}\rvert$
26	0.78±0.07	1.30±0.11	0.48±0.13
28	0.93±0.09	1.22±0.10	0.20±0.14
29	1.02±0.10	1.17±0.10	0.15±0.14
30	1.09±0.10	1.13±0.10	0.03±0.14
31	1.17±0.10	1.08±0.10	0.09±0.14
32	1.24±0.12	1.03±0.09	0.21±0.14
34	1.39±0.13	0.94±0.08	0.45±0.15

TABLE III. Critical exponent γ for gas and liquid phases for different choices of trial value of critical point m_c at energy 4.0 GeV/nucleon used in γ matching procedure. Normalized moments.

Trial m_c	γ_{liquid}	γ_{gas}	$\lvert\gamma_{gas}-\gamma_{liquid}\rvert$
26	0.83±0.09	1.32±0.09	0.49±0.13
28	1.01±0.11	1.22±0.09	0.21±0.14
29	1.10±0.12	1.17±0.08	0.08±0.14
30	1.18±0.13	1.12±0.08	0.06±0.14
31	1.27±0.14	1.07±0.08	0.20±0.15
32	1.35±0.15	1.01±0.07	0.33±0.16
34	1.52±0.16	0.91±0.07	0.61±0.17

TABLE IV. Critical exponent γ for gas and liquid phases for different choices of trial value of critical point m_c at energy 4.0 GeV/nucleon used in gamma matching procedure. Non-normalized moments.

Trial m_c	γ_{liquid}	γ_{gas}	$\lvert\gamma_{gas}-\gamma_{liquid}\rvert$
26	0.77±0.07	1.53±0.08	0.75±0.11
28	0.96±0.08	1.42±0.07	0.46±0.11
29	1.05±0.09	1.36±0.07	0.31±0.11
30	1.13±0.09	1.30±0.07	0.17±0.11
31	1.22±0.09	1.24±0.07	0.02±0.11
32	1.30±0.10	1.18±0.06	0.13±0.12
34	1.47±0.11	1.06±0.06	0.41±0.14

and $48 \leqslant m \leqslant 67$ for the gas phase. Although the variation of Z_{A_0} is considerable, especially in the gas region, the variation of the second charge moment is much smaller, since the normalized M_2 depends on $\ln Z_{A_0}$. On the other hand, the pre-equilibrium particles (more numerous in the gas phase) are omitted from calculation of normalized moments. Thus, the variation of Z_{A_0} is compensated by exclusion of the pre-equilibrium particles, resulting in similar values of normalized and non-normalized moments.

The analogous results of the γ matching procedure at energy 4.0 GeV/nucleon are given in Tables III and IV. The determined critical point is $m_c=30\pm2$ and the critical exponent $\gamma=1.15\pm0.09$. Figure 13 shows values of $\lvert\gamma_{liquid}-\gamma_{gas}\rvert$ plotted as a function of trial values of critical multiplicity at energy 10.6 GeV/nucleon. Figure 14 presents results of fitting procedure for γ_{liquid} and γ_{gas} for critical multiplicity value $m_c=30$ at the same energy.

VI. CRITICAL EXPONENTS β AND τ

After determination of the critical multiplicity m_c and ranges of ϵ in which to fit the critical exponents, determination of the exponents β and τ is straightforward. Based on Eq. (5), the mean value of $\ln Z_{max}$ was plotted as a function of $\ln\lvert m-m_c\rvert$ (Fig. 15). The slope of the linear fit to the plotted

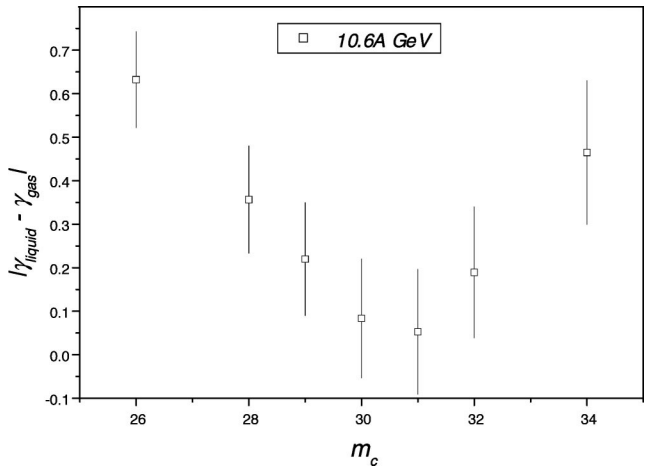

FIG. 13. Difference $\lvert\gamma_{liquid}-\gamma_{gas}\rvert$ as a function of trial multiplicity m_c at energy 10.6 GeV/nucleon.

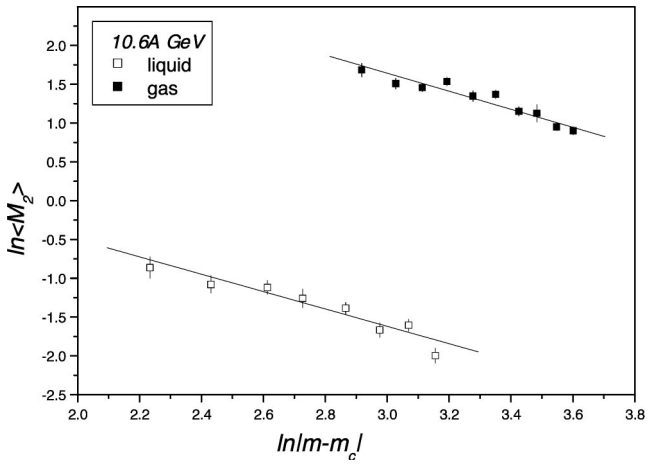

FIG. 14. Mean value of second charge moment $\langle M_2\rangle$ for a liquid and gas as a function of multiplicity m at energy 10.6 GeV/nucleon. The plotted lines show fits to experimental data used to determine critical exponent γ.

relation gives the critical exponent β. A linear fit was made within the fitting boundaries determined during the γ matching procedure. At energy 10.6 GeV/nucleon, the determined value of $\beta=0.33\pm0.01$ with $\chi^2/ndf=1.66$, and at 4.0 GeV/nucleon, $\beta=0.34\pm0.01$ with $\chi^2/ndf=0.99$.

The critical exponent τ was determined from the equation [7,15]

$$\frac{\Delta \ln\langle M_3\rangle}{\Delta \ln\langle M_2\rangle} = \frac{\tau-4}{\tau-3}. \tag{9}$$

Figure 16 presents $\ln\langle M_3\rangle$ versus $\ln\langle M_2\rangle$ for the gas phase at energy 10.6 GeV/nucleon together with the linear fit. The slope of this linear fit is used to determine the τ exponent, which is $\tau=2.11\pm0.05$ at 10.6 GeV/nucleon and $\tau=2.12\pm0.04$ at energy 4.0 GeV/nucleon. The τ exponent was calculated based on data from the gas phase. Although Eq. (9) is valid on both sides of the critical point, the effects due to finite (and small) size of the system are enhanced in the liquid phase. We keep in mind that Z_{max} is

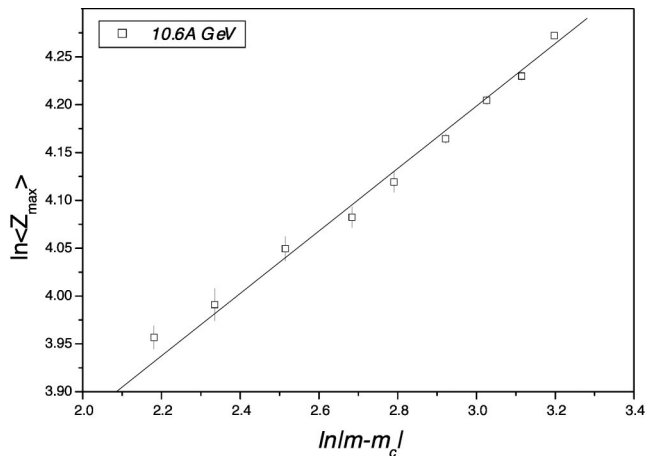

FIG. 15. Mean value of $\ln\langle Z_{max}\rangle$ as a function of distance from critical point ϵ for the liquid phase at 10.6 GeV/nucleon.

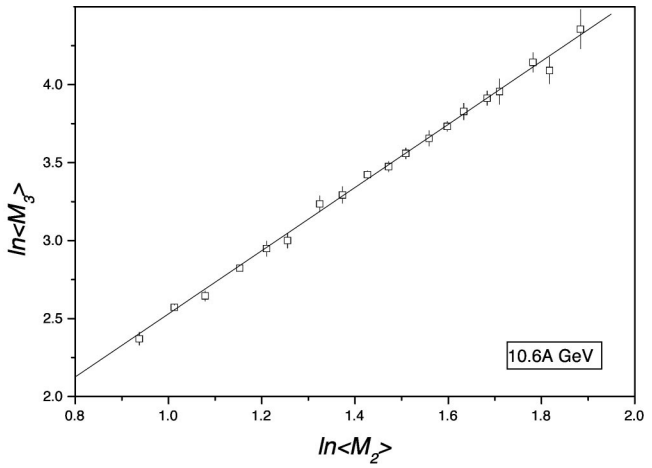

FIG. 16. Relation between charge moments $\ln\langle M_3\rangle$ and $\ln\langle M_3\rangle$ for the gas phase at 10.6 GeV/nucleon.

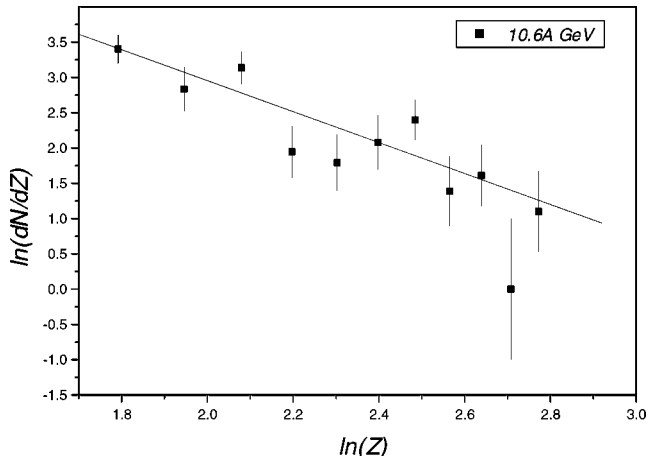

FIG. 17. Normalized fragment charge distribution in events with multiplicity m within the range $25<m<35$.

excluded from M_2 calculation in the liquid phase and thus there are only very few fragments left in the calculation, resulting in altering the calculated value of the τ exponent [22]. Therefore, it is a common practice to calculate τ based on data in the gas phase only [8,23,10].

To verify the consistency of the exponent τ determination, the τ was also calculated from Eq. (4). This equation is supposed to be valid at the critical point, but in order to have sufficient statistics, data with $25<m<35$ were used. Normalized charge distribution was calculated and plotted in Fig. 17. The exponent τ is given by the slope of the linear fit to the data points for charges from $Z=6$ to $Z=16$. For charges smaller than 6, the assumptions of the Fisher model are not valid [24] and for charges larger than 16 the experimental data statistics is too small. The resulting value $\tau=2.19\pm0.33$, with reduced $\chi^2=1.2$, is in agreement with the previously determined value.

VII. DISCUSSION

Table V summarizes the values of critical exponents γ, β, and τ at energies 4.0 and 10.6 GeV/nucleon, both for normalized and non-normalized charge moments, determined in this work. For comparison, exponents obtained by the EOS, EMU01, and KLMM experiments are also shown, as well as the values predicted by the liquid-gas and percolation models. The data on the β and γ exponents from Table V are plotted in Fig. 18. The values of β and γ exponents determined in this work are very close to those expected for the "liquid-gas" phase transition, both for 4.0 and 10.6 GeV/nucleon data. We note that the critical exponents discussed here were determined from the selected liquid and gas groups of events. Earlier analyses, without such a selection, gave values of the exponents which do not agree with any of the models.

Values of the critical exponent τ predicted by the percolation and liquid-gas models are not too different. As experimental errors are large compared to the difference between the predicted values of τ, this exponent cannot be used to discriminate models of multifragmentation.

Presented in this work a suggestion that the Fisher's liquid drop model properly describes the multifragmentation process, is in agreement with recently published results of the ISiS Collaboration [21], confirming that the Fisher's scaling law is followed by experimental data. In addition, Mader *et al.* [25] have shown a similarity between predictions based on the Fisher model and clusterization process in the three-dimensional Ising model, so that droplet condensation and $d=3$ Ising belong to the same universality class. Therefore, multifragmentation can be interpreted in a similar way as

TABLE V. Critical exponents γ, β, τ at energies 4.0 and 10.6 GeV/nucleon obtained in this work, compared with the results from other experiments and with model predictions.

Data	γ	β	τ
Au-Em 4.0*A* GeV norm	1.15±0.09	0.34±0.01	2.12±0.04
Au-Em 10.6*A* GeV norm	1.17±0.09	0.33±0.01	2.11±0.05
Au-Em 4.0*A* GeV	1.23±0.09	0.36±0.02	2.15±0.04
Au-Em 10.6*A* GeV	1.11±0.09	0.33±0.02	2.16±0.05
Au-C 1.0*A* GeV (EOS [15])	1.40±0.10	0.29±0.02	2.14±0.06
Au-Em 10.6*A* GeV (EMU01 [10])	0.86±0.05	0.25±0.02	2.23±0.05
Au-Em 10.6*A* GeV (KLMM [8])		0.19±0.02	1.88±0.06
$d=3$ Ising (liquid-gas)	1.23	0.33	2.21
$d=3$ percolation	1.80	0.41	2.18

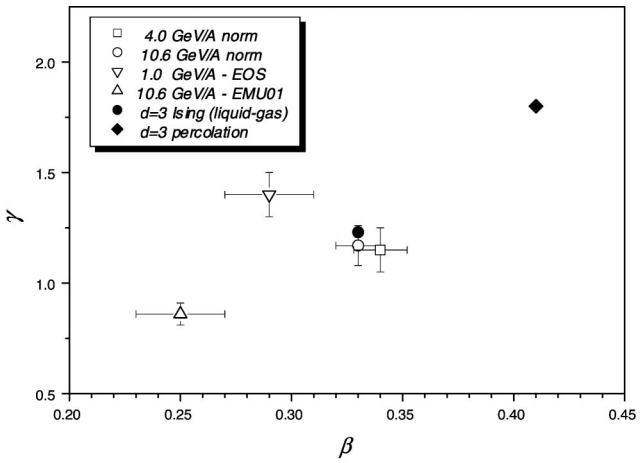

FIG. 18. Comparison of determined and predicted values of critical exponents γ and β.

condensation of liquid drops in equilibrium with the bulk liquid.

One can try to estimate a critical temperature of the system by using a relation between multiplicity and temperature of the system given in Refs. [3,6]. Estimation of the initial temperature of the system after collision, T_i, was based on Fermi gas model and did not take into account the expansion of the system. The final temperature of the system at breakup, T_f, was estimated based on a relation between multiplicity m and temperature T for isotopic-yield-ratio thermometer given in Ref. [3]. Our values of critical multiplicity (m_c=30 and m_c=31 at 4.0 and 10.6 GeV/nucleon, respectively) correspond to T_i=9.3±0.7 MeV and T_f =5.4±0.2 MeV. The error of T_i reflects uncertainty of the input parameters in the Fermi gas model. The T_i and T_f values bracket the critical temperature of the system. This estimated range for the critical temperature is comparable with theoretical estimates for small nuclear systems [26,27] and with results obtained in Ref. [21]. The estimation of the critical temperature relies on the assumption that relation between multiplicity m and temperature of the system established for energy 1.0A GeV applies also for higher energies 4.0 and 10.6 GeV/nucleon.

The above results, together with results of the ISiS Collaboration [21], suggest that not all multifragmentation events undergo a second-order phase transition. In Refs. [5] and [21] the ISiS data were shown to undergo a first-order phase transition ending at a critical point. The data in this paper show the same behavior. For $|m-m_c|>0$ the system is away from the critical point. For $m-m_c<0$ the system is below the critical point and would undergo a first-order phase transition. Only at $m=m_c$, or when M_2 diverges, or Z_{max} vanishes, is the system at its critical point and undergoes a continuous (second-order) phase transition.

As noted earlier, the excited nucleus after a collision evolves into the neighborhood of the critical point on the density-temperature plane. If multifragmentation occurs close to the critical point, critical exponents characterizing second-order phase transition occurring in the neighborhood of the critical point should be observed. If for some events multifragmentation occurs far away from the critical point and they are included in the analysis, the observed values of critical exponents could be altered so that the whole picture of the physical process is obscured. In such situations a proper selection of events should help obtain true values of critical exponents.

Events excluded from our analysis show very strong fluctuations of the second moment of the charge distribution significantly far away from the critical point, especially in the liquid phase. Large fluctuations could result from coexistence of two different phases with different properties inside a single nucleus. Below critical multiplicity m_c (proportional to temperature of the system) two separate phases with significantly different properties could coexist in nucleus as is suggested by mean field [28,29,1] or canonical model calculations [30]. The coexistence of the two phases may take place in wide ranges of temperature and pressure. This could explain large fluctuations of second moment of charge distribution far away from the critical point. It is also important to stress that moment M_2 is proportional to the isothermal compressibility of the system. Therefore, large fluctuations of M_2 correspond to fluctuations of the compressibility κ_T and to fluctuation of the density of the system. Large fluctuations of M_2 observed in liquid phase (Fig. 4) may be interpreted as resulting from large density difference between the two coexisting phases.

In summary, an attempt to extract critical exponents γ, β, and τ was performed, using data coming from interactions of gold nuclei with nuclear emulsion at energies 4.0A GeV and 10.6A GeV. To extract the exponents, two subsets of data with characteristics similar to that of gas and liquid phases were selected, based on analysis of Campi's second charge moments. The extracted values of the critical exponents for the selected datasets are in agreement with predictions of liquid-gas model of phase transition. The same analysis performed without the selection of gas and liquid samples favors neither percolation nor liquid-gas model of phase transition. A suggestion is made that data excluded from the above mentioned samples represent events in which phase transition, if any, occurs far from the critical point.

ACKNOWLEDGMENTS

We thank our colleagues from the Kraków-Louisiana-Minnesota Collaboration for the effort of obtaining data on angular distributions of gold interaction events at 10.6 GeV/nucleon, which were used in this study. We also thank Professor C. J. Waddington for taking care of emulsion irradiation to the 4 GeV/nucleon gold beam at the AGS accelerator at BNL.

[1] T. Sil *et al.*, Phys. Rev. C **63**, 054604 (2001).
[2] J. Pochodzalla *et al.*, Phys. Rev. Lett. **75**, 1040 (1995).
[3] J. Hauger *et al.*, Phys. Rev. Lett. **77**, 235 (1996).
[4] R. Nebauer and J. Aichelin, Nucl. Phys. **A681**, 353 (2001).
[5] M. K. Berkenbusch *et al.*, Phys. Rev. Lett. **88**, 022701 (2002).
[6] J. A. Hauger *et al.*, Phys. Rev. C **57**, 764 (1998).
[7] M. L. Gilkes *et al.*, Phys. Rev. Lett. **73**, 1590 (1994).
[8] M. L. Cherry *et al.*, Phys. Rev. C **52**, 2652 (1995).
[9] M. I. Adamovitch *et al.*, Eur. Phys. J. A **1**, 77 (1998).
[10] M. I. Adamovitch. *et al.*, Eur. Phys. J. A **5**, 429 (1999).
[11] X. Campi, J. Phys. A **19**, L917 (1986).
[12] D. Stauffer and A. Aharony, *Introduction to Percolation Theory*, 2nd ed. (Taylor and Francis, London, 1988).
[13] W. Bauer and W. A. Friedman, Phys. Rev. Lett. **75**, 767 (1995).
[14] W. Bauer and A. Botvina, Phys. Rev. C **52**, R1760 (1995).
[15] J. B. Elliott *et al.*, Phys. Rev. C **62**, 064603 (2000).
[16] D. Kudzia *et al.*, Nucl. Instrum. Methods Phys. Res. A **431**, 252 (1999).
[17] C. F. Powell, P. H. Fowler, and D. H. Perkins, *The Study of Elementary Particles by the Photographic Method* (Pergamon, New York, 1959).
[18] X. Campi, Phys. Lett. B **208**, 351 (1988).
[19] M. E. Fisher, Physics (Long Island City, N.Y.) **3**, 255 (1967).
[20] W. Bauer, Phys. Rev. C **38**, 1297 (1988).
[21] J. B. Elliott *et al.*, Phys. Rev. Lett. **88**, 042701 (2002).
[22] J. B. Elliott *et al.*, Phys. Rev. C **49**, 3185 (1988).
[23] P. L. Jain and G. Singh, Phys. Lett. B **382**, 289 (1996).
[24] A. D. Panagiotou *et al.*, Phys. Rev. C **31**, 55 (1985).
[25] C. M. Mader *et al.*, nucl-th/0103030.
[26] H. R. Jaqaman *et al.*, Phys. Rev. C **29**, 2067 (1984).
[27] P. Bonche *et al.*, Nucl. Phys. **A436**, 265 (2002).
[28] J. N. De *et al.*, Phys. Rev. C **55**, R1641 (1997).
[29] J. N. De, B. K. Agrawal, and S. K. Samaddar, Phys. Rev. C **59**, R1 (1999).
[30] S. J. Lee and A. Z. Mekjan, Phys. Rev. C **56**, 2621 (1997).